COMMUN. MATH. SCI.
Vol. 10, No. 4, pp. 1081–1103

A CONTINUUM MODEL FOR THE DYNAMICS OF DISLOCATION ARRAYS*

XIAOHONG ZHU† AND YANG XIANG‡

Abstract. We derive a continuum model for the dynamics of a dislocation array that consists of dislocations in different slip planes. In the continuum model, the dislocation array is represented by a continuous surface, of which there are many dislocations in a unit area at the scale of the continuum model. The continuum model is derived rigorously from the discrete model of the dynamics of the constituent dislocations in the array using asymptotic analysis. The obtained continuum model contains an integral over the dislocation array surface representing the long-range interaction of dislocations, and a local term that comes from the line tension effect of dislocations. The size-dependent effect due to dislocation line tension is accurately incorporated in the continuum model. Well-posedness of the continuum model is examined. A generalization to dislocation arrays in an elastically anisotropic medium is discussed.

Key words. Dislocation dynamics, Peach-Koehler force, continuum model, elasticity, plasticity.

AMS subject classifications. 35Q74, 74A10, 74A50.

1. Introduction

Dislocations are line defects and the primary carriers of plastic deformation in crystalline materials [15]. In plastic deformation processes, dislocations are commonly observed to form wall structures such as arrays and networks. Thus these dislocation structures play important roles in plastic behaviors of crystalline materials. Many theoretical and experimental results can be found in the literature on these dislocation structures, e.g., structures and dynamics of low angle grain boundaries modeled by arrays or networks of dislocations [33, 42, 21, 36, 15, 41, 44, 7, 23], interaction of dislocation walls with solutes [43] and particles [8], formation of the dislocation cell-wall structures and implications of these structures in cyclically deformed FCC metals [26, 16, 25, 22], and propagation of shear bands modeled by interaction of tilt walls of dislocation arrays with particles [14, 34].

The main difficulty in the modeling and simulation of dislocation arrays and other structures comes from the multiscale nature of dislocations: on one hand, the interaction of dislocations is long-range; and on the other hand, there are many short-range interactions such as self-force, annihilation, reaction, and multiplication that play important roles in the evolution of dislocation microstructures [15]. Dislocations interact and move under the force associated with the stress field in the medium referred to as the Peach-Koehler force [15, 30]. In equilibrium states without other effects, the constituent dislocations in the arrays are straight and the surfaces spanned by the dislocation arrays are planar. For such arrays of straight dislocations, analytical formulas for the force and energy are available, e.g., in the dislocation model of planar low

*Received: October 24, 2011; accepted (in revised form): January 31, 2012. Communicated by Weinan E.
This work was partially supported by the Hong Kong Research Grants Council General Research Fund 605410, the Fundamental Research Funds for the Central Universities of China, and Product Research and Development Program of Ministry of Education and Guangdong Province under Grant 2011B090400458.

†Department of Mathematics, Jinan University, Guangzhou 510632, China (zhuxiaohong@gmail.com).
‡Department of Mathematics, The Hong Kong University of Science and Technology, Clear Water Bay, Kowloon, Hong Kong (maxiang@ust.hk).

angle grain boundaries consisting of straight dislocations [33, 15, 41] and interaction between solutes and walls of straight dislocations [43].

In reality, the constituent dislocations in dislocation arrays and the surfaces spanned by the dislocation arrays are commonly curved during dynamical processes or when interacting with other defects such as external dislocations or particles. Using dislocation models, thermal fluctuations in low angle grain boundaries were analyzed [36]. For walls of curved dislocations, local line tension approximation [14] and approximation of the curved dislocations with a few straight segments [34] were used for a uniform finite edge dislocation array bypassing particles. Calculations of the stress fields of uniform dislocation arrays with three-dimensional perturbations were performed in [32]. The stress fields of disordered and finite dislocation walls were studied in [38]. The stabilizing force on perturbed grain boundaries was analyzed by using a dislocation model in [54]. Migration of low angle grain boundaries in the presence of extrinsic dislocations was studied in [23]. Interactions of dislocation arrays with particles were simulated in [8]. Loss of interface coherency around a misfitting inclusion was examined by using a dislocation model in [31]. In these studies, except for some special dislocation array configurations, numerical methods are employed to obtain the interactions among all the constituent dislocations in the arrays and/or with other defects.

At large length and time scales, continuum models are desired for the modeling and simulation of collective behaviors of dislocation ensembles. The continuum models for dislocation dynamics and plasticity available in the literature are based on continuous distributions of dislocations, neglecting the details of motion and interactions of individual dislocations [27, 17, 28, 2, 9, 35, 29, 13, 1, 4, 12, 39, 50, 40, 18]. While the long-range interaction of dislocations is relatively well-modeled within these continuum models [27, 17], a major challenge is how to incorporate various dislocation short-range interactions into the continuum framework. These available continuum models incorporate the short-range interactions, if at all, only phenomenologically or in some average senses, and are not able to accurately reflect the dislocation structures of dislocation arrays. For example, it has been shown that a recent continuum model derived from statistical distributions of dislocations [12] does not apply to some special arrangement of dislocations in the dislocation walls [37]. In our previous papers [46, 53] we have attempted to derive accurate continuum models for the Peach-Koehler force and dislocation dynamics in a single slip plane. As far as we know, no continuum model is available in the literature for the general arrays or network structures of dislocations in three dimensions such as the low angle grain boundaries and the dislocation walls discussed above.

Under the Peach-Koehler force, dislocations move by glide in their own slip planes except at high temperatures, which is widely adopted in discrete dislocation dynamics simulations (e.g. [19, 51, 11, 47, 3]). For examples of dislocation arrays, it has been analyzed by theories and observed in experiments that grain boundaries may form [6, 5] and migrate [42, 21] by dislocation glide at low temperatures; dislocation walls bypassing particles via dislocation glide have been studied by using discrete dislocation dynamics simulations [14, 34, 8].

In this paper, we present a continuum model for the dynamics of dislocation arrays in three dimensions (equations (3.1) and (3.4), see also figure 2.1 for an illustrative plot of such a dislocation array). In this continuum model, the dislocation array is represented by a continuous surface in three dimensions, of which there are many dislocations in a unit area at the length scale of the continuum model. The

continuum formula of the force on this surface in an elastically isotropic medium is derived rigorously from the discrete model of the Peach-Koehler force on the constituent dislocations in the array in the continuum regime. The obtained continuum force contains an integral over the surface representing the long-range interaction of dislocations in the array, and a local term that comes from the local line tension effect of the constituent dislocations. Well-posedness of this continuum model is established through linear stability analysis of regular dislocation arrays. By an example of dislocation arrays around an obstacle, it is also shown that the continuum model accurately retains the size-dependent nature of dislocation arrays, which is missing in the continuum theories containing only the long-range dislocation interaction. Generalization to dislocation arrays in an elastically anisotropic medium is discussed.

The rest of the paper is organized as follows. In Section 2, we review the discrete model for the dynamics of dislocations in a dislocation array, from which our continuum model is derived. In Section 3, we present our continuum model and summarize its main features. In Section 4, we present the details of the derivation of a continuum approximation for the Peach-Koehler force from the discrete model using asymptotic analysis. In Section 5, we examine the well-posedness of the continuum model by linear stability analysis of regular dislocation arrays. In Section 6, we examine the accuracy of the continuum model by an example and show that the continuum model correctly retains the size-dependent effect. In Section 7, a generalization of the formulation to the context of elastically anisotropic media is discussed.

2. Elasticity theory and the discrete model

In this section, we briefly review the discrete model for the dynamics of a dislocation array, from which our continuum model will be derived.

We consider an array of dislocations γ_j, $j=\cdots,-2,-1,0,1,2,\cdots$ with the same Burgers vector and lying in parallel equidistant slip planes; see figure 2.1. Without loss of generality, we choose the normal direction of the slip planes to be the z direction. The Burgers vector of the dislocations is $\mathbf{b}=(b_1,b_2,0)$. The distance between two adjacent slip planes is D, which is of order of the length of the Burgers vector $b=\sqrt{b_1^2+b_2^2}$, and $\frac{b}{D}$ is a small finite number. For example, for a low angle symmetric tilt boundary consisting of a regular array of straight edge dislocations, $\theta=\frac{b}{D}$ is the tilt angle and $\theta\leq\frac{\pi}{12}$ ([33], [15] Chap. 19, [41] Chap. 2). We neglect the effect of dislocation climb, thus these dislocations can only glide in their own slip planes. We consider the dislocation array in the bulk of the material and assume that the dislocation array is unbounded, thus the boundary effects due to the image force and finite size of the array are neglected.

We first briefly review the linear elasticity theory in the presence of dislocations ([15], part I). The elastic displacement $\mathbf{u}$ has an increment of the Burgers vector $\mathbf{b}$ along any loop L enclosing a dislocation:

$$\oint_L d\mathbf{u}=\mathbf{b}. \tag{2.1}$$

This equation can be rewritten in terms of the distortion tensor $\mathbf{w}$, where $w_{ij}=\partial u_j/\partial x_i$ for $i,j=1,2,3$, as

$$\nabla\times\mathbf{w}=\mathbf{t}\delta_\gamma\otimes\mathbf{b}, \tag{2.2}$$

where $\mathbf{t}$ is the unit tangent vector of the dislocation, δ_γ is the Dirac delta function of the dislocation, and the operator $\otimes$ denotes the tensor product of two vectors. The

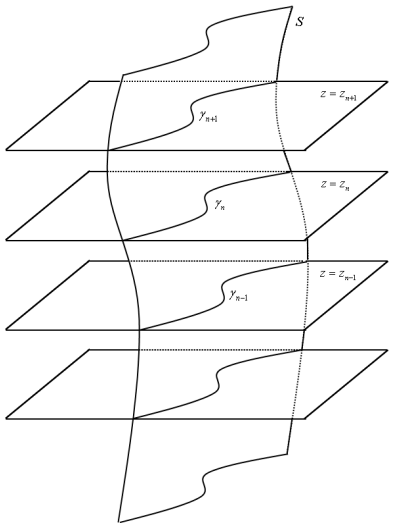

FIG. 2.1. *A schematic plot of a dislocation array. The array consists of dislocations γ_j in the slip plane $z = z_j$, $j = \cdots, -2, -1, 0, 1, 2, \cdots$. S is the surface spanned by the dislocation array, which is used to represent the dislocation array in the continuum model.*

strain tensor is given by

$$\epsilon_{ij} = \frac{1}{2}(w_{ij} + w_{ji}) \tag{2.3}$$

for $i, j = 1, 2, 3$. The stress tensor σ is determined from the strain tensor by the linear elastic constitutive equations

$$\sigma_{ij} = \sum_{k,l=1}^{3} C_{ijkl}\epsilon_{kl} \tag{2.4}$$

for $i, j = 1, 2, 3$, where $\{C_{ijkl}\}$ is the elastic constant tensor. For an isotropic medium, the constitutive equations can be written as

$$\sigma_{ij} = 2\mu\epsilon_{ij} + \mu\frac{2\nu}{1-2\nu}(\epsilon_{11} + \epsilon_{22} + \epsilon_{33})\delta_{ij} \tag{2.5}$$

for $i, j = 1, 2, 3$, where μ is the shear modulus, ν is the Poisson ratio, and δ_{ij} is equal to 1 if $i = j$ and is equal to 0 otherwise. In the absence of body forces, the equilibrium equation is

$$\nabla \cdot \sigma = \mathbf{0}. \tag{2.6}$$

The Peach-Koehler force on a dislocation due to the stress field in the medium is ([30], and equation (4-43) in Section 4.6 in [15]):

$$\mathbf{F} = \sigma \cdot \mathbf{b} \times \mathbf{t}. \tag{2.7}$$

For the dislocation array, under isotropic elasticity, at a point $\mathbf{X} = (x, y, z_n)$ on the dislocation γ_n in the array, it can be calculated from the analytical formula of the

stress field associated with dislocations ([15], equation (4-31) in Section 4.4), that the Peach-Koehler force in the slip plane in the normal direction of the dislocation γ_n is

$$f^d(\mathbf{X}) = \sum_{j\neq n}\int_{\gamma_j}\left[\frac{\mu b^2}{4\pi}\frac{\mathbf{r}_j\cdot\mathbf{n}_j}{\|\mathbf{r}_j\|^3} + \frac{\nu\mu}{4\pi(1-\nu)}\frac{(\mathbf{n}_j\cdot\mathbf{b})(\mathbf{r}_j\cdot\mathbf{b})}{\|\mathbf{r}_j\|^3} - \frac{3\mu}{4\pi(1-\nu)}\frac{(z_j-z_n)^2(\mathbf{n}_j\cdot\mathbf{b})(\mathbf{r}_j\cdot\mathbf{b})}{\|\mathbf{r}_j\|^5}\right]ds$$
$$+\int_0^{+\infty}\int_0^{2\pi}\eta\delta(\eta,\psi)d\eta d\psi\int_{\gamma_n^{\eta,\psi}}\left[\frac{\mu b^2}{4\pi}\frac{\mathbf{r}_{\eta,\psi}\cdot\mathbf{n}_{\eta,\psi}}{\|\mathbf{r}_{\eta,\psi}\|^3} + \frac{\nu\mu}{4\pi(1-\nu)}\frac{(\mathbf{n}_{\eta,\psi}\cdot\mathbf{b})(\mathbf{r}_{\eta,\psi}\cdot\mathbf{b})}{\|\mathbf{r}_{\eta,\psi}\|^3}\right.$$
$$\left. - \frac{3\mu}{4\pi(1-\nu)}\frac{(z_{\eta,\psi}-z_n)^2(\mathbf{n}_{\eta,\psi}\cdot\mathbf{b})(\mathbf{r}_{\eta,\psi}\cdot\mathbf{b})}{\|\mathbf{r}_{\eta,\psi}\|^5}\right]ds, \tag{2.8}$$

where μ is the shear modulus, ν is the Poisson ratio, $\mathbf{r}_j = \mathbf{X}-\mathbf{X}_j$, $\mathbf{X}_j = (x_j, y_j, z_j)$ is a point on the dislocation γ_j, $\mathbf{n}_j = \mathbf{n}_j(\mathbf{X}_j)$ is the unit normal vector of the dislocation γ_j at the point $\mathbf{X}_j$, and ds is the element of the line integral along γ_j. Here the normal direction of a dislocation is defined by $\mathbf{n}_s \times \mathbf{t}$, where $\mathbf{n}_s$ is the unit vector in the z direction and $\mathbf{t}$ is the dislocation line direction. The summation of integrals in f^d gives the force from all other dislocations. The last integral in f^d is the force due to the stress generated by γ_n itself, in which

$$\gamma_n^{\eta,\psi} = \{(x_{\eta,\psi}, y_{\eta,\psi}, z_{\eta,\psi}) = (x_1, y_1, z_n) + \eta\cos\psi\mathbf{n}_n(\mathbf{X}_1) + (0,0,\eta\sin\psi) : \mathbf{X}_1 = (x_1, y_1, z_n) \in \gamma_n\}, \tag{2.9}$$

where $\mathbf{n}_{\eta,\psi}$ is the unit normal vector of $\gamma_n^{\eta,\psi}$, $\mathbf{r}_{\eta,\psi} = \mathbf{X} - \mathbf{X}_{\eta,\psi}$ with $\mathbf{X}_{\eta,\psi} \in \gamma_n^{\eta,\psi}$, and δ is a regularized delta function of the dislocation γ_n defined in the plane perpendicular to γ_n and expressed in terms of the polar coordinates with radius η and angle ψ. See figure 2.2 for an illustration of the point $\mathbf{X}_{\eta,\psi} \in \gamma_n^{\eta,\psi}$.

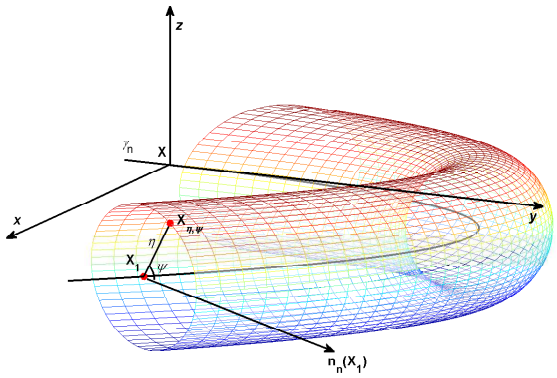

FIG. 2.2. *A point $\mathbf{X}_{\eta,\psi} \in \gamma_n^{\eta,\psi}$ defined in equation (2.9) in the vicinity of dislocation γ_n. Here (η,ψ) is the polar coordinate defined in the plane perpendicular to γ_n, with η being the radius and ψ being the angle with respect to the unit normal vector $\mathbf{n}_n$ of γ_n. This parametrization is used in the expression of the self force of dislocation γ_n; see equation (2.8).*

The regularized delta function δ removes the singularity in the line integral along γ_n itself, and physically represents the distribution of the Burgers vector within the dislocation core whose width is of the order of the length of the Burgers vector b. This

is one of the standard treatments in the dislocation theory to remove the unphysical singularities caused by the breakdown of the linear elasticity theory within the dislocation core region [15](Chap. 8) and [20, 17, 24, 47, 3]. In this paper, we assume that the regularized delta function of the dislocation core has compact support within the core and is radially symmetric: $\delta = \delta(\eta)$.

In discrete dislocation dynamics simulations (e.g. [19, 51, 11, 47, 3]), the dislocations glide in their own slip planes with normal velocity

$$v = Mf^d, \tag{2.10}$$

where v is the velocity of the dislocation, and M is the mobility.

3. The continuum model

In this section, we present the continuum model for the dynamics of dislocation arrays, which is derived from the above discrete dislocation model in equations (2.8) and (2.10).

In the continuum model, a dislocation array is represented by the continuous surface S spanned by the dislocation lines contained in the array; see figure 2.1. A constituent dislocation γ_j in the array is then the intersection of the dislocation array surface S and the plane $z = z_j$, for $j = \cdots, -2, -1, 0, 1, 2, \cdots$. In the derivation, we assume that in the length unit of the continuum model, the length of the Burgers vector is $b = \|\mathbf{b}\| \ll 1$, and there are many dislocations in a unit area of the continuum model. We also assume that the curvature radii of the constituent dislocations and the geodesics perpendicular to the dislocations are both O(1) in the length unit of the continuum model.

The obtained continuum model for the glide Peach-Koehler force on the constituent dislocations is

$$\begin{aligned} f(\mathbf{X}) = \frac{1}{D}\int_S \Big[& \frac{\mu b^2}{4\pi}\frac{\mathbf{r}\cdot\tilde{\mathbf{n}}_d(\mathbf{X}^S)}{\|\mathbf{r}\|^3} + \frac{\nu\mu}{4\pi(1-\nu)}\frac{(\tilde{\mathbf{n}}_d(\mathbf{X}^S)\cdot\mathbf{b})(\mathbf{r}\cdot\mathbf{b})}{\|\mathbf{r}\|^3} \\ & - \frac{3\mu}{4\pi(1-\nu)}\frac{(\mathbf{r}\cdot\mathbf{n}_s)^2(\tilde{\mathbf{n}}_d(\mathbf{X}^S)\cdot\mathbf{b})(\mathbf{r}\cdot\mathbf{b})}{\|\mathbf{r}\|^5}\Big] dS \\ & + \frac{\mu b^2}{4\pi(1-\nu)}\kappa\Bigg\{ \big(1+\nu-3\nu\sin^2\beta\big)\log\frac{D}{2\pi r_c\|\tilde{\mathbf{n}}_d\|} - \frac{3}{2} + \frac{\nu}{2} + \left(\frac{5}{4}-\frac{\nu}{2}\right)\sin^2\beta \\ & + [3-\nu+(-1+\nu)\sin^2\beta]\|\tilde{\mathbf{n}}_d\|^2 - 2\|\tilde{\mathbf{n}}_d\|^4\sin^2\beta\Bigg\}, \end{aligned} \tag{3.1}$$

where the force is at a point $\mathbf{X}$ on the dislocation array surface S in the normal direction of the constituent dislocation, which is defined as the intersection line of the dislocation array surface and the slip plane of the dislocation, $\mathbf{X}^S$ is a point on the dislocation array surface S, $\mathbf{r} = \mathbf{X} - \mathbf{X}^S$, dS is the surface element, $\mathbf{n}_{\text{surface}}$ is the normal direction of the dislocation array surface, $\mathbf{n}_s$ is the normal direction of the slip planes of the constituent dislocations,

$$\tilde{\mathbf{n}}_d = \mathbf{n}_{\text{surface}} - (\mathbf{n}_{\text{surface}}\cdot\mathbf{n}_s)\mathbf{n}_s \tag{3.2}$$

is the component of $\mathbf{n}_{\text{surface}}$ in the normal direction of the constituent dislocation, κ is the curvature of the constituent dislocation, β is the angle between the constituent dislocation and its Burgers vector, and r_c is a parameter depending on the dislocation core:

$$\log r_c = \int_0^{+\infty}\int_0^{2\pi} \eta\delta(\eta,\psi)\log\eta\, d\eta d\psi. \tag{3.3}$$

Accordingly, the velocity of the dislocation array surface in the continuum model, from equation (2.10), is

$$\mathbf{v} = Mf\frac{\tilde{\mathbf{n}}_d}{\|\tilde{\mathbf{n}}_d\|}. \tag{3.4}$$

Note that this velocity is in the normal direction of the constituent dislocation in its slip plane.

The integral term in our continuum model in equation (3.1) gives the long-range interaction of dislocations in the array. The local term in it gives correction due to the dislocation line tension effect. It is widely known that the line tension effect of dislocations, which is an important short-range effect and may lead to size dependent properties, is missing in the integral models for the interaction of continuous distributions of dislocations [28, 2, 35, 39, 50, 40, 18, 46, 53]. Here we give an accurate expression without an adjustable parameter for this line tension effect for dislocations in a three dimensional array, which is not available in the literature to the best of our knowledge.

The details of the derivation using asymptotic analysis is presented in Section 4. As the length of the Burgers vector $b \to 0$ in the length unit in the continuum model, we keep the $O(1)$ integral term representing the long-range interaction of dislocations and terms at $O(b\log b)$ coming from the line tension effect of the dislocations. We also keep those $O(b)$ terms due to dislocation line tension in the continuum model to incorporate the complete contribution from the dislocation line tension effect. It will be shown in Section 5 by linear stability analysis that the obtained continuum model is well-posed and is very accurate as an approximation to the discrete model in the continuum regime. The size effect of the dislocation interaction is correctly incorporated in the continuum model, as will be shown by an example in Section 6.

In addition to those $O(b)$ terms due to dislocation line tension, it is tempting to include all the rest $O(b)$ terms to increase the accuracy of the continuum model. However, these terms other than the line tension effect at $O(b)$ will lead to ill-posedness of the continuum model. Alternatively, one can try to solve this problem of ill-posedness by including even higher order terms in the continuum model. However, this alternative method will make the expression extremely complicated and will involve even higher derivatives, resulting in severe stability restrictions on the time steps (the CFL condition) in numerical simulations. We choose not to include these terms in the continuum model. More discussion can be found in Section 5.

Finally, a generalization of the formulation to the context of elastically anisotropic media will be discussed in Section 7.

4. Derivation of the continuum approximation

In this section, we present the derivation of the continuum Peach-Koehler force on the dislocation array from the discrete dislocation model by using asymptotic analysis.

4.1. Outline of the derivation. For convenience of derivation, we assume that the dislocation array surface S is smooth. The dislocation γ_j in the slip plane $z = z_j$ is the intersection of the surface S and the plane $z = z_j = jD$, for $j = \cdots, -2, -1, 0, 1, 2, \cdots$.

We will derive a continuum model from the discrete model given in equation (2.8). The derivation method is a generalization of those used to obtain continuum models for the Peach-Koehler force on dislocations in a single slip plane [46, 53] and the elastic interaction on epitaxial surfaces [45, 48, 49, 55].

First of all, the discrete model $f^d(\mathbf{X})$ in equation (2.8) for the Peach-Koehler force on the point $\mathbf{X}\in\gamma_n$ can be written as

$$f^d(\mathbf{X})=\sum_{j\neq n}h(\mathbf{X},z_j)+I_1(\mathbf{X},z_n,h), \tag{4.1}$$

where $h(\mathbf{X},z_j)$ is the integral along γ_j given by

$$h(\mathbf{X},z_j)=\int_{\gamma_j}\left[\frac{\mu b^2}{4\pi}\frac{\mathbf{r}_j\cdot\mathbf{n}_j}{\|\mathbf{r}_j\|^3}+\frac{\nu\mu}{4\pi(1-\nu)}\frac{(\mathbf{n}_j\cdot\mathbf{b})(\mathbf{r}_j\cdot\mathbf{b})}{\|\mathbf{r}_j\|^3}-\frac{3\mu}{4\pi(1-\nu)}\frac{(z_j-z_n)^2(\mathbf{n}_j\cdot\mathbf{b})(\mathbf{r}_j\cdot\mathbf{b})}{\|\mathbf{r}_j\|^5}\right]ds, \tag{4.2}$$

and $I_1(\mathbf{X},z_n,h)$ is the integral around γ_n given by

$$\begin{aligned}I_1(\mathbf{X},z_n,h)=\int_0^{+\infty}\int_0^{2\pi}\eta\delta(\eta,\psi)d\eta d\psi\int_{\gamma_n^{\eta,\psi}}&\left[\frac{\mu b^2}{4\pi}\frac{\mathbf{r}_{\eta,\psi}\cdot\mathbf{n}_{\eta,\psi}}{\|\mathbf{r}_{\eta,\psi}\|^3}+\frac{\nu\mu}{4\pi(1-\nu)}\frac{(\mathbf{n}_{\eta,\psi}\cdot\mathbf{b})(\mathbf{r}_{\eta,\psi}\cdot\mathbf{b})}{\|\mathbf{r}_{\eta,\psi}\|^3}\right.\\&\left.-\frac{3\mu}{4\pi(1-\nu)}\frac{(z_{\eta,\psi}-z_n)^2(\mathbf{n}_{\eta,\psi}\cdot\mathbf{b})(\mathbf{r}_{\eta,\psi}\cdot\mathbf{b})}{\|\mathbf{r}_{\eta,\psi}\|^5}\right]ds,\end{aligned} \tag{4.3}$$

where $\gamma_n^{\eta,\psi}$ is a line near γ_n defined in equation (2.9).

The discrete summation in equation (4.1) can be regarded as a numerical scheme of the integral

$$f^0(\mathbf{X})=\frac{1}{D}\int_{-\infty}^{+\infty}h(\mathbf{X},z)dz, \tag{4.4}$$

where

$$h(\mathbf{X},z)=\int_{\gamma_z}\left[\frac{\mu b^2}{4\pi}\frac{\mathbf{r}_z\cdot\mathbf{n}_z}{\|\mathbf{r}_z\|^3}+\frac{\nu\mu}{4\pi(1-\nu)}\frac{(\mathbf{n}_z\cdot\mathbf{b})(\mathbf{r}_z\cdot\mathbf{b})}{\|\mathbf{r}_z\|^3}-\frac{3\mu}{4\pi(1-\nu)}\frac{(z-z_n)^2(\mathbf{n}_z\cdot\mathbf{b})(\mathbf{r}_z\cdot\mathbf{b})}{\|\mathbf{r}_z\|^5}\right]ds, \tag{4.5}$$

the curve $\gamma_z=\{(x,y,z)\in S:\text{any } x,y\}$, $\mathbf{r}_z=\mathbf{X}-\mathbf{X}_z$, $\mathbf{X}_z=(x_z,y_z,z)$ is a point on the curve γ_z, and $\mathbf{n}_z$ is the unit normal vector of γ_z. Thus, the integral expression $f^0(\mathbf{X})$ in equation (4.4) gives a leading order approximation of the discrete model in equation (4.1), and it can be written as

$$\begin{aligned}f^0(\mathbf{X})=\frac{1}{D}\int_S\Big[&\frac{\mu b^2}{4\pi}\frac{\mathbf{r}\cdot\tilde{\mathbf{n}}_d(\mathbf{X}^S)}{\|\mathbf{r}\|^3}+\frac{\nu\mu}{4\pi(1-\nu)}\frac{(\tilde{\mathbf{n}}_d(\mathbf{X}^S)\cdot\mathbf{b})(\mathbf{r}\cdot\mathbf{b})}{\|\mathbf{r}\|^3}\\&-\frac{3\mu}{4\pi(1-\nu)}\frac{(\mathbf{r}\cdot\mathbf{n}_s)^2(\tilde{\mathbf{n}}_d(\mathbf{X}^S)\cdot\mathbf{b})(\mathbf{r}\cdot\mathbf{b})}{\|\mathbf{r}\|^5}\Big]dS.\end{aligned} \tag{4.6}$$

However, it is widely known that the line tension effect of dislocations, which is an important short-range effect and may lead to size dependent properties, is missing in the integral models for the interaction of continuous distributions of dislocations [28, 2, 35, 39, 50, 40, 18]. Except for the accurate continuum models we obtained previously for distributions of dislocations in a single slip plane [46, 53] (which do not apply here), the available models incorporating this local line tension effect all contain adjustable parameters and the forms of the additional local terms do not agree with one another.

Mathematically, the above discussion indicates that the integral approximation in equation (4.4) is not good enough for the discrete summation in equation (4.1). This problem is caused by the singularity in the integrand $h(\mathbf{X},z)$ of the integral in equation (4.4). In order to obtain more accurate continuum approximation, we shall keep the leading order error terms of the integral approximation in equation (4.4) in

the continuum model. For this purpose, we need the following asymptotic behavior near the singularity of $h(\mathbf{X},z)$ and the theorem on the error estimate associated with singular integrand.

Asymptotic Behavior of the Integrand $h(\mathbf{X},z)$. From the asymptotic behavior of the self-stress of a dislocation [52], when $\mathbf{X}$ is very close to γ_z, i.e., $z\to z_n$, we have

$$h(\mathbf{X},z)=\frac{\mu b^2}{2\pi}\left(1-\sin^2\beta+\frac{1}{1-\nu}\sin^2\beta\cos 2\tilde{\theta}\right)\cos\tilde{\theta}\frac{1}{d} -\frac{\mu b^2}{4\pi(1-\nu)}(1+\nu-3\nu\sin^2\beta)\kappa\log d+O(1), \tag{4.7}$$

where β is the angle between the Burgers vector $\mathbf{b}$ and the line direction of the dislocation γ_n at the point $\mathbf{X}$, $\tilde{\theta}$ is the angle between the vector $(\mathbf{X}-\mathbf{X}_z^0)$ and the normal direction of the curve γ_z at the point $\mathbf{X}_z^0$ where $(\mathbf{X}-\mathbf{X}_z^0)\perp\gamma_z$, $d=O(z-z_n)$ is the distance between the point $\mathbf{X}$ and the curve γ_z, and κ is the curvature of the dislocation γ_n at the point $\mathbf{X}$.

Error Estimate Theorem [49]. Suppose that interval $[a_1,a_2]$ is divided into m subintervals with $\Delta x=(a_2-a_1)/m$, $x_j=a_1+(j-1)\Delta x$, $j=1,\cdots,m+1$. Let $G(x)=g_1(x)\log|x-t|+g_2(x)/(x-t)+g_3(x)$ with $t=x_{j_0}$ for some j_0, where $g_1(x)$, $g_2(x)$, and $g_3(x)$ are twice continuously differentiable functions. Then

$$\int_{a_1}^{a_2}G(x)\,dx=\Delta x\left(\frac{G(a_1)+G(a_2)}{2}+\sum_{2\le j\le m,j\neq j_0}G(x_j)\right) +\int_{t-\frac{\Delta x}{2}}^{t+\frac{\Delta x}{2}}G(x)\,dx-(\log\pi-1)g_1(t)\Delta x+O((\Delta x)^2). \tag{4.8}$$

Applying the above theorem and the asymptotic behavior of $h(\mathbf{X},z)$ to the integral with respect to z in equation (4.4), with $\Delta z=D=O(b)$, we have

$$f^d(\mathbf{X})=f^0(\mathbf{X})-(\log\pi-1)\frac{\mu b^2}{4\pi(1-\nu)}(1+\nu-3\nu\sin^2\beta)\kappa+I_1-I_2+O(b^3), \tag{4.9}$$

where I_1 is defined in equation (4.3), and I_2 is an integral (corresponding to the term $\int_{t-\frac{\Delta x}{2}}^{t+\frac{\Delta x}{2}}G(x)\,dx$ in equation (4.8) in the above theorem) given by

$$I_2=\frac{1}{D}\int_{z_n-\frac{D}{2}}^{z_n+\frac{D}{2}}dz\int_{\gamma_z}\Big[\frac{\mu b^2}{4\pi}\frac{\mathbf{r}_z\cdot\mathbf{n}_z}{\|\mathbf{r}_z\|^3}+\frac{\nu\mu}{4\pi(1-\nu)}\frac{(\mathbf{n}_z\cdot\mathbf{b})(\mathbf{r}_z\cdot\mathbf{b})}{\|\mathbf{r}_z\|^3} -\frac{3\mu}{4\pi(1-\nu)}\frac{(z-z_n)^2(\mathbf{n}_z\cdot\mathbf{b})(\mathbf{r}_z\cdot\mathbf{b})}{\|\mathbf{r}_z\|^5}\Big]ds. \tag{4.10}$$

The remaining task is to find the leading order terms of the difference of the two integrals in the above equation: I_1-I_2, which will be done in the rest of this section. In particular, in Subsection 3.2, we reformulate the two integrals; in Subsection 3.3, we calculate the asymptotic behavior of I_1-I_2; finally, in Subsection 3.4, we summarize the result of the asymptotic behavior.

4.2. Reformulation of the two integrals. In order to calculate the difference between the two integrals I_1 and I_2 in equations (4.3) and (4.10), respectively, we first rewrite both of them as line integrals along the dislocation γ_n in this subsection.

Suppose that γ_n is parameterized by its arc length s. The unit tangent vector and unit normal vector at a point $\mathbf{X}_1(s)=(x_1(s),y_1(s),z_n)\in\gamma_n$ are

$$\mathbf{t}(\mathbf{X}_1)=(x_1'(s),y_1'(s),0) \tag{4.11}$$

and

$$\mathbf{n}(\mathbf{X}_1)=(-y_1'(s),x_1'(s),0), \tag{4.12}$$

respectively.

The first integral I_1 in equation (4.3) comes from the self force of dislocation γ_n. The curve $\gamma_n^{\eta,\psi}$ (defined in equation (2.9)) in it can also be parameterized by s (no longer arc length) as

$$\mathbf{X}_{\eta,\psi}=(x_{\eta,\psi}(s),y_{\eta,\psi}(s),z_{\eta,\psi})=(x_1(s)-\eta\cos\psi y_1'(s),y_1(s)+\eta\cos\psi x_1'(s),z_n+\eta\sin\psi) \tag{4.13}$$

(see also figure 2.2), and its tangent vector and normal vector (not normalized) are $\mathbf{t}_{\eta,\psi}(\mathbf{X}_{\eta,\psi})=(1-\eta\cos\psi\kappa(s))\mathbf{t}(\mathbf{X}_1)$ and $\mathbf{n}_{\eta,\psi}(\mathbf{X}_{\eta,\psi})=(1-\eta\cos\psi\kappa(s))\mathbf{n}(\mathbf{X}_1)$, respectively, where $\kappa(s)$ is the curvature of γ_n at point $\mathbf{X}_1(s)$. Note that $(x_1''(s),y_1''(s),0)=\kappa(s)(-y_1'(s),x_1'(s),0)$. Thus we can rewrite I_1 in equation (4.3) as

$$\begin{aligned} I_1=\int_0^{+\infty}\int_0^{2\pi}\eta\delta(\eta,\psi)d\eta d\psi\int_{\gamma_n}(1-\eta\cos\psi\kappa(s))\\ \times\left[\frac{\mu b^2}{4\pi}\frac{\mathbf{r}_{\eta,\psi}\cdot\mathbf{n}(\mathbf{X}_1)}{\|\mathbf{r}_{\eta,\psi}\|^3}+\frac{\nu\mu}{4\pi(1-\nu)}\frac{(\mathbf{n}(\mathbf{X}_1)\cdot\mathbf{b})(\mathbf{r}_{\eta,\psi}\cdot\mathbf{b})}{\|\mathbf{r}_{\eta,\psi}\|^3}\right.\\ \left.-\frac{3\mu}{4\pi(1-\nu)}\frac{\eta^2\sin^2\psi(\mathbf{n}(\mathbf{X}_1)\cdot\mathbf{b})(\mathbf{r}_{\eta,\psi}\cdot\mathbf{b})}{\|\mathbf{r}_{\eta,\psi}\|^5}\right]ds, \end{aligned} \tag{4.14}$$

where $\mathbf{r}_{\eta,\psi}=\mathbf{X}-\mathbf{X}_{\eta,\psi}$.

We then rewrite the second integral I_2 in equation (4.10) also as an integral along the dislocation γ_n. When $z\in\left[z_n-\frac{D}{2},z_n+\frac{D}{2}\right]$, the curve γ_z can be parameterized by the arc length s of γ_n in the following way: for a given point $\mathbf{X}_1(s)=(x_1(s),y_1(s),z_n)\in\gamma_n$, we determine a point $\mathbf{X}_z(s)=(x_z(s),y_z(s),z)\in\gamma_z$ such that $\mathbf{X}_z-\mathbf{X}_1$ is normal to γ_n at $\mathbf{X}_1$, by

$$\mathbf{X}_z(s)=\mathbf{X}_1(s)+A(\mathbf{X}_1,z)\mathbf{n}(\mathbf{X}_1)+(0,0,z-z_n), \tag{4.15}$$

where the coefficient $A(\mathbf{X}_1,z)$ will be determined in the next subsection. See figure 4.1 for an illustration of this expression for $\mathbf{X}_z(s)$. We then have

$$\mathbf{r}_z=\mathbf{X}-\mathbf{X}_z=\mathbf{X}-\mathbf{X}_1-A(\mathbf{X}_1,z)\mathbf{n}(\mathbf{X}_1)-(0,0,z-z_n), \tag{4.16}$$

$$\mathbf{n}_z=\frac{1}{\sqrt{x_z'(s)^2+y_z'(s)^2}}\left[(1-A(\mathbf{X}_1,z)\kappa(\mathbf{X}_1))\mathbf{n}(\mathbf{X}_1)-\frac{\partial A(\mathbf{X}_1,z)}{\partial s}\mathbf{t}(\mathbf{X}_1)\right], \tag{4.17}$$

and

$$A(\mathbf{X}_1,z),\ \frac{\partial A(\mathbf{X}_1,z)}{\partial s}=O(z-z_n)=O(D)=O(b),\quad z\in\left[z_n-\frac{D}{2},z_n+\frac{D}{2}\right]. \tag{4.18}$$

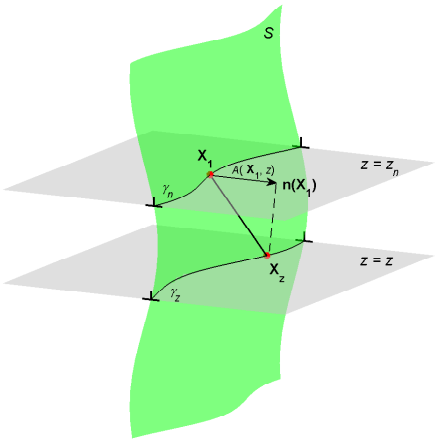

FIG. 4.1. *A point* $\mathbf{X}_z(s)$ *on a nearby dislocation* γ_z *is expressed in terms of* $\mathbf{X}_1(s)$ *on the dislocation* γ_n *and the normal direction* $\mathbf{n}(\mathbf{X}_1)$ *of* γ_n*; see equation (4.15). This expression is used in the new formulation of* I_2 *in equation (4.19).*

Thus I_2 in equation (4.10) can be written as

$$I_2 = \frac{1}{D}\int_{z_n-\frac{D}{2}}^{z_n+\frac{D}{2}} dz \int_{\gamma_n} \Bigg\{ (1-A(\mathbf{X}_1,z)\kappa(\mathbf{X}_1)) \Big[\frac{\mu b^2}{4\pi} \frac{\mathbf{r}_z\cdot\mathbf{n}(\mathbf{X}_1)}{\|\mathbf{r}_z\|^3} + \frac{\nu\mu}{4\pi(1-\nu)} \frac{(\mathbf{n}(\mathbf{X}_1)\cdot\mathbf{b})(\mathbf{r}_z\cdot\mathbf{b})}{\|\mathbf{r}_z\|^3} - \frac{3\mu}{4\pi(1-\nu)} \frac{(z-z_n)^2(\mathbf{n}(\mathbf{X}_1)\cdot\mathbf{b})(\mathbf{r}_z\cdot\mathbf{b})}{\|\mathbf{r}_z\|^5} \Big] - \frac{\partial A(\mathbf{X}_1,z)}{\partial s} \Big[\frac{\mu b^2}{4\pi} \frac{\mathbf{r}_z\cdot\mathbf{t}(\mathbf{X}_1)}{\|\mathbf{r}_z\|^3} + \frac{\nu\mu}{4\pi(1-\nu)} \frac{(\mathbf{t}(\mathbf{X}_1)\cdot\mathbf{b})(\mathbf{r}_z\cdot\mathbf{b})}{\|\mathbf{r}_z\|^3} - \frac{3\mu}{4\pi(1-\nu)} \frac{(z-z_n)^2(\mathbf{t}(\mathbf{X}_1)\cdot\mathbf{b})(\mathbf{r}_z\cdot\mathbf{b})}{\|\mathbf{r}_z\|^5} \Big] \Bigg\} ds. \tag{4.19}$$

4.3. Difference between I_1 and I_2. In this subsection, we calculate the difference between the integrals I_1 and I_2, given in equations (4.14) and (4.19), respectively.

We use a shifted arc length parameter s for the dislocation γ_n with $\mathbf{X} = (x, y, z_n) = \gamma_n(0)$. Let γ_n^A be the segment of γ_n for $s \in [-b^\alpha, b^\alpha]$ with $0 < \alpha < \frac{1}{2}$, and let $\gamma_n^B = \gamma_n - \gamma_n^A$. We first consider I_1 and I_2 on γ_n^B. Under the given assumptions, we have

$$\|\mathbf{X} - \mathbf{X}_1\| \geq \frac{1}{2} b^\alpha, \quad \mathbf{X}_1 \in \gamma_n^B. \tag{4.20}$$

Thus when $\mathbf{X}_1 \in \gamma_n^B$ and $\eta = O(b)$, from equations (2.9) and (4.20) we have

$$\mathbf{r}_{\eta,\psi} = \mathbf{X} - \mathbf{X}_{\eta,\psi} = \mathbf{X} - \mathbf{X}_1 - \eta[\cos\psi \mathbf{n}(\mathbf{X}_1) + (0,0,\sin\psi)] = \mathbf{r}\left(1 + O(b^{1-\alpha})\right), \tag{4.21}$$

where $\mathbf{r} = \mathbf{X} - \mathbf{X}_1$. Using equations (4.20) and (4.21), when the inner line integral is along γ_n^B in I_1 in equation (4.14), and $\eta = O(b)$, we have

$$I_1^B = \int_{\gamma_n^B} \left[\frac{\mu b^2}{4\pi} \frac{\mathbf{r}\cdot\mathbf{n}}{\|\mathbf{r}\|^3} + \frac{\nu\mu}{4\pi(1-\nu)} \frac{(\mathbf{n}\cdot\mathbf{b})(\mathbf{r}\cdot\mathbf{b})}{\|\mathbf{r}\|^3} \right] ds + O(b^{3-3\alpha}). \tag{4.22}$$

Similarly, for the integral I_2 given by equation (4.19) on γ_n^B, using equation (4.16) and $D=O(b)$, we have

$$\mathbf{r}_z=\mathbf{r}\left(1+O(b^{1-\alpha})\right) \tag{4.23}$$

and

$$I_2^B=\int_{\gamma_n^B}\left[\frac{\mu b^2}{4\pi}\frac{\mathbf{r}\cdot\mathbf{n}}{\|\mathbf{r}\|^3}+\frac{\nu\mu}{4\pi(1-\nu)}\frac{(\mathbf{n}\cdot\mathbf{b})(\mathbf{r}\cdot\mathbf{b})}{\|\mathbf{r}\|^3}\right]ds+O(b^{3-3\alpha}). \tag{4.24}$$

We then consider I_1 and I_2 on γ_n^A. When $\mathbf{X}_1\in\gamma_n$ is close to $\mathbf{X}$,

$$\mathbf{X}_1=\mathbf{X}+\left(s-\frac{1}{6}\kappa^2s^3\right)\mathbf{t}^0+\left(\frac{1}{2}\kappa s^2+\frac{1}{6}\kappa' s^3\right)\mathbf{n}^0+O(s^4), \tag{4.25}$$

where $\mathbf{t}^0$ is the unit tangent vector of γ_n at point $\mathbf{X}$, $\mathbf{n}^0$ is the unit normal vector of γ_n at point $\mathbf{X}$, κ is the curvature of γ_n at $\mathbf{X}$, and $\kappa'=\frac{d\kappa(s)}{ds}\Big|_{s=0}$. Then the unit tangent vector, unit normal vector, and curvature at $\mathbf{X}_1$ are

$$\mathbf{t}(\mathbf{X}_1)=\left(1-\frac{1}{2}\kappa^2s^2\right)\mathbf{t}^0+\left(\kappa s+\frac{1}{2}\kappa' s^2\right)\mathbf{n}^0+O(s^3), \tag{4.26}$$

$$\mathbf{n}(\mathbf{X}_1)=\left(-\kappa s-\frac{1}{2}\kappa' s^2\right)\mathbf{t}^0+\left(1-\frac{1}{2}\kappa^2s^2\right)\mathbf{n}^0+O(s^3), \tag{4.27}$$

and

$$\kappa(\mathbf{X}_1)=\kappa+O(s), \tag{4.28}$$

respectively. We also denote

$$\mathbf{b}/b=b_1^0\mathbf{t}^0+b_2^0\mathbf{n}^0=\cos\beta\ \mathbf{t}^0+\sin\beta\ \mathbf{n}^0. \tag{4.29}$$

Recall that β is the angle between the Burgers vector $\mathbf{b}$ and the dislocation line direction $\mathbf{t}^0$.

For the integral I_1 in equation (4.14) on γ_n^A, we have

$$\begin{aligned}
I_1^A=\int_0^{+\infty}\int_0^{2\pi}\eta\delta(\eta,\psi)d\eta d\psi\int_{-b^\alpha}^{b^\alpha}\Bigg\{&\frac{\mu b^2}{4\pi}\left[\frac{\frac{1}{2}\kappa s^2-\eta\cos\psi+\kappa\eta^2\cos^2\psi}{(s^2+\eta^2)^{3/2}}-\frac{\frac{3}{2}\kappa\eta^2s^2\cos^2\psi}{(s^2+\eta^2)^{5/2}}\right]\\
&+\frac{\nu\mu b^2}{4\pi(1-\nu)}\left[\frac{-b_1^0b_2^0s-(b_2^0)^2\eta\cos\psi+3\kappa b_1^0b_2^0\eta s\cos\psi+\kappa\left[(b_1^0)^2-\frac{1}{2}(b_2^0)^2\right]s^2}{(s^2+\eta^2)^{3/2}}\right.\\
&\qquad\left.+\frac{\kappa(b_2^0)^2\eta^2\cos^2\psi}{(s^2+\eta^2)^{3/2}}+\frac{-\frac{3}{2}\kappa b_1^0b_2^0\eta s^3\cos\psi-\frac{3}{2}\kappa(b_2^0)^2\eta^2s^2\cos^2\psi}{(s^2+\eta^2)^{5/2}}\right]\\
&-\frac{3\mu b^2}{4\pi(1-\nu)}\left[\frac{-b_1^0b_2^0\eta^2s\sin^2\psi-(b_2^0)^2\eta^3\sin^2\psi\cos\psi+3\kappa b_1^0b_2^0\eta^3s\sin^2\psi\cos\psi}{(s^2+\eta^2)^{5/2}}\right.\\
&\qquad+\frac{\kappa\left[(b_1^0)^2-\frac{1}{2}(b_2^0)^2\right]\eta^2s^2\sin^2\psi+\kappa(b_2^0)^2\eta^4\sin^2\psi\cos^2\psi}{(s^2+\eta^2)^{5/2}}\\
&\qquad\left.-\frac{\frac{5}{2}\kappa b_1^0b_2^0\eta^3s^3\sin^2\psi\cos\psi+\frac{5}{2}\kappa(b_2^0)^2\eta^4s^2\sin^2\psi\cos^2\psi}{(s^2+\eta^2)^{7/2}}\right]+O(b^2)\Bigg\}ds
\end{aligned}$$

$$
\begin{aligned}
&= \int_0^{+\infty}\int_0^{2\pi} \eta\delta(\eta,\psi)d\eta d\psi \Bigg\{ \frac{\mu b^2}{4\pi}\left[\kappa\big(\log(2b^\alpha)-\log\eta-1+\cos^2\psi\big)-\frac{2\cos\psi}{\eta}\right] \\
&\quad + \frac{\nu\mu}{4\pi(1-\nu)}\left[(b_2^0)^2\left(\kappa\cos^2\psi-\frac{2\cos\psi}{\eta}\right)+\kappa\big(2(b_1^0)^2-(b_2^0)^2\big)\big(\log(2b^\alpha)-1-\log\eta\big)\right] \\
&\quad - \frac{\mu}{4\pi(1-\nu)}\Bigg[4(b_2^0)^2\left(\kappa\sin^2\psi\cos^2\psi-\frac{\sin^2\psi\cos\psi}{\eta}\right)+\kappa\big(2(b_1^0)^2-(b_2^0)^2\big)\sin^2\psi \\
&\qquad\qquad -2\kappa(b_2^0)^2\sin^2\psi\cos^2\psi\Bigg]+O(b^{2+\alpha})\Bigg\}. \qquad (4.30)
\end{aligned}
$$

Note that since δ is a two-dimensional regularized delta function, $\int_0^{+\infty}\int_0^{2\pi}\eta\delta(\eta,\psi)d\eta d\psi = 1$.

If $\delta(\eta,\psi)$ is independent of the angle ψ, i.e., $\delta(\eta,\psi)=\delta(\eta)$, we have

$$
\begin{aligned}
I_1^A &= \frac{\mu b^2}{4\pi}\kappa\left(\log\frac{2b^\alpha}{r_c}-\frac{1}{2}\right) \\
&\quad + \frac{\mu}{4\pi(1-\nu)}\kappa\left[\nu\big(2(b_1^0)^2-(b_2^0)^2\big)\log\frac{2b^\alpha}{r_c}-\nu\left(2(b_1^0)^2-\frac{3}{2}(b_2^0)^2\right)-(b_1^0)^2+\frac{1}{4}(b_2^0)^2\right] \\
&\quad + O(b^{2+\alpha}), \qquad (4.31)
\end{aligned}
$$

where r_c is a parameter depending on the dislocation core given in equation (3.3).

Next we calculate the integral I_2 in equation (4.19) on γ_n^A. Using the arclength s of γ_n and z for the parametrization of the dislocation array S, as given in equation (4.15), when $z\in[z_n-\frac{D}{2},z_n+\frac{D}{2}]$ and $s\in[-b^\alpha,b^\alpha]$, the surface S can be written as

$$
y^0 = \frac{\kappa}{2}(x^0)^2+\frac{1}{2}\kappa_n(1+A_1^2)^{3/2}(z^0)^2+A_2x^0z^0+A_1z^0+O((x^0)^3+(z^0)^3), \qquad (4.32)
$$

where $(x^0,y^0,z^0=z-z_n)$ is the coordinate of a point $\mathbf{X}_z$ on the surface S in the coordinate system $\{\mathbf{t}^0,\mathbf{n}^0,\mathbf{n}_s=(0,0,1)\}$ at the point $\mathbf{X}$, κ_n is the normal curvature of the surface S in the direction perpendicular to the dislocation γ_n,

$$
A_1(\mathbf{X}) = \frac{\mathbf{n}_{\text{surface}}(\mathbf{X})\cdot\mathbf{n}_s}{\|\tilde{\mathbf{n}}_d(\mathbf{X})\|}, \qquad (4.33)
$$

and

$$
A_2(\mathbf{X}) = \left.\frac{\partial^2\mathbf{X}_z}{\partial\mathbf{t}^0\partial\mathbf{n}_s}\right|_{\mathbf{X}}\cdot\mathbf{n}^0. \qquad (4.34)
$$

Recall that $\mathbf{n}_{\text{surface}}$ is the unit normal vector of the dislocation array surface S, $\mathbf{n}_s$ is the unit normal vector of the slip planes of the dislocations, and $\tilde{\mathbf{n}}_d$ is the component of $\mathbf{n}_{\text{surface}}$ in the normal direction of the constituent dislocation given in equation (3.2). Note that A_2 is associated with the variation of the dislocation line direction, in the direction normal to the slip plane. It can be calculated from equations (4.15), (4.25), and (4.32) that

$$
A(\mathbf{X}_1,z) = A_1(z-z_n)+A_2s(z-z_n)+\frac{1}{2}\kappa_n(1+A_1^2)^{3/2}(z-z_n)^2+O(s^3+(z-z_n)^3). \qquad (4.35)
$$

Then I_2 in equation (4.19) on γ_n^A can be written as

$$
\begin{aligned}
I_2^A = \frac{1}{D}\int_{z_n-\frac{D}{2}}^{z_n+\frac{D}{2}} dz \int_{-b^\alpha}^{b^\alpha} \Bigg\{ & \\
& \frac{\mu b^2}{4\pi}\left[\frac{-A_1(z-z_n)+\frac{1}{2}\kappa s^2 - A_2 s(z-z_n)+\left(-\frac{\kappa_n(1+A_1^2)^{3/2}}{2}+A_1^2\kappa\right)(z-z_n)^2}{\left(s^2+(1+A_1^2)(z-z_n)^2\right)^{3/2}}\right. \\
& \left. -\frac{\frac{3}{2}A_1^2\kappa s^2(z-z_n)^2 - 3A_1^2A_2 s(z-z_n)^3 - \frac{3}{2}A_1^2\kappa_n(1+A_1^2)^{3/2}(z-z_n)^4}{\left(s^2+(1+A_1^2)(z-z_n)^2\right)^{5/2}}\right] \\
& + \frac{\nu\mu b^2}{4\pi(1-\nu)}\left[\frac{-b_1^0b_2^0 s-(b_2^0)^2A_1(z-z_n)+\left(3b_1^0b_2^0A_1\kappa-(b_2^0)^2A_2\right)s(z-z_n)}{\left(s^2+(1+A_1^2)(z-z_n)^2\right)^{3/2}}\right. \\
& + \frac{\left((b_1^0)^2-\frac{1}{2}(b_2^0)^2\right)\kappa s^2+(b_2^0)^2\left(-\frac{\kappa_n(1+A_1^2)^{3/2}}{2}+A_1^2\kappa\right)(z-z_n)^2}{\left(s^2+(1+A_1^2)(z-z_n)^2\right)^{3/2}} \\
& - \frac{\frac{3}{2}b_1^0b_2^0A_1\kappa s^3(z-z_n)+\left(\frac{3}{2}(b_2^0)^2A_1^2\kappa-3b_1^0b_2^0A_1A_2\right)s^2(z-z_n)^2}{\left(s^2+(1+A_1^2)(z-z_n)^2\right)^{5/2}} \\
& \left. + \frac{3A_1\left((b_2^0)^2A_1A_2+b_1^0b_2^0\frac{\kappa_n(1+A_1^2)^{3/2}}{2}\right)s(z-z_n)^3+\frac{3}{2}(b_2^0)^2A_1^2\kappa_n(1+A_1^2)^{3/2}(z-z_n)^4}{\left(s^2+(1+A_1^2)(z-z_n)^2\right)^{5/2}}\right] \\
& - \frac{3\mu b^2}{4\pi(1-\nu)}\left[\frac{-b_1^0b_2^0 s(z-z_n)^2-(b_2^0)^2A_1(z-z_n)^3+\left(3b_1^0b_2^0A_1\kappa-(b_2^0)^2A_2\right)s(z-z_n)^3}{\left(s^2+(1+A_1^2)(z-z_n)^2\right)^{5/2}}\right. \\
& + \frac{\left((b_1^0)^2-\frac{1}{2}(b_2^0)^2\right)\kappa s^2(z-z_n)^2+(b_2^0)^2\left(-\frac{\kappa_n(1+A_1^2)^{3/2}}{2}+A_1^2\kappa\right)(z-z_n)^4}{\left(s^2+(1+A_1^2)(z-z_n)^2\right)^{5/2}} \\
& - \frac{\frac{5}{2}b_1^0b_2^0A_1\kappa s^3(z-z_n)^3+\left(\frac{5}{2}(b_2^0)^2A_1^2\kappa-5b_1^0b_2^0A_1A_2\right)s^2(z-z_n)^4}{\left(s^2+(1+A_1^2)(z-z_n)^2\right)^{7/2}} \\
& \left. + \frac{\left(5(b_2^0)^2A_1^2A_2+\frac{5}{2}b_1^0b_2^0A_1\kappa_n(1+A_1^2)^{3/2}\right)s(z-z_n)^5+\frac{5}{2}(b_2^0)^2A_1^2\kappa_n(1+A_1^2)^{3/2}(z-z_n)^6}{\left(s^2+(1+A_1^2)(z-z_n)^2\right)^{7/2}}\right] \\
& + \frac{\mu b^2}{4\pi}\left[\frac{A_2 s(z-z_n)}{\left(s^2+(1+A_1^2)(z-z_n)^2\right)^{3/2}}\right] + \frac{\nu\mu b^2}{4\pi(1-\nu)}\left[\frac{(b_1^0)^2A_2 s(z-z_n)+b_1^0b_2^0A_1A_2(z-z_n)^2}{\left(s^2+(1+A_1^2)(z-z_n)^2\right)^{3/2}}\right] \\
& - \frac{3\mu b^2}{4\pi(1-\nu)}\left[\frac{(b_1^0)^2A_2 s(z-z_n)^3+b_1^0b_2^0A_1A_2(z-z_n)^4}{\left(s^2+(1+A_1^2)(z-z_n)^2\right)^{5/2}}\right]+O(b^2)\Bigg\}ds \\
= & \frac{\mu b^2}{4\pi}\kappa\left(\log\frac{4b^\alpha}{D}-\log\sqrt{1+A_1^2}\right)+\frac{\nu\mu b^2}{4\pi(1-\nu)}\kappa\left(2(b_1^0)^2-(b_2^0)^2\right)\left(\log\frac{4b^\alpha}{D}-\log\sqrt{1+A_1^2}\right) \\
& + \frac{\mu b^2}{4\pi}\left[\frac{-\kappa_n(1+A_1^2)^{3/2}+A_1^2\kappa}{1+A_1^2}+\frac{2A_1^2\kappa_n}{\sqrt{1+A_1^2}}\right] \\
& + \frac{\nu\mu b^2}{4\pi(1-\nu)}\left[\frac{-(b_2^0)^2\kappa_n(1+A_1^2)^{3/2}+2b_1^0b_2^0A_1A_2+(b_2^0)^2A_1^2\kappa}{1+A_1^2}+\frac{2(b_2^0)^2A_1^2\kappa_n}{\sqrt{1+A_1^2}}\right] \\
& - \frac{\mu b^2}{4\pi(1-\nu)}\left[\frac{-2(b_2^0)^2\kappa_n(1+A_1^2)^{3/2}+4b_1^0b_2^0A_1A_2+2(b_2^0)^2A_1^2\kappa}{(1+A_1^2)^2}+\frac{2(b_1^0)^2-(b_2^0)^2}{1+A_1^2}\kappa\right.
\end{aligned}
$$

$$+\frac{8(b_2^0)^2A_1^2\kappa_n}{(1+A_1^2)^{3/2}}\Bigg]+\frac{\mu b^2}{4\pi(1-\nu)}b_1^0b_2^0A_1A_2\left[\frac{2\nu}{1+A_1^2}-\frac{4}{(1+A_1^2)^2}\right]+O(b^{2+\alpha}). \tag{4.36}$$

Therefore, the difference $I_1-I_2=(I_1^A-I_2^A)+(I_1^B-I_2^B)$ can be calculated from equations (4.22), (4.24), (4.31), and (4.36).

4.4. The continuum approximation. Using equations (4.4), (4.5), (4.9), (4.22), (4.24), (4.31), and (4.36), and letting $\alpha=1/4$, the continuum approximation of $f^d(\mathbf{X})$, keeping the terms of the leading two orders as $b\to 0$, written in a parametrization-independent form, is

$$\begin{aligned}
&f^c(\mathbf{X})\\
&=\frac{1}{D}\int_S\Bigg[\frac{\mu b^2}{4\pi}\frac{\mathbf{r}\cdot\tilde{\mathbf{n}}_d(\mathbf{X}^S)}{\|\mathbf{r}\|^3}+\frac{\nu\mu}{4\pi(1-\nu)}\frac{(\tilde{\mathbf{n}}_d(\mathbf{X}^S)\cdot\mathbf{b})(\mathbf{r}\cdot\mathbf{b})}{\|\mathbf{r}\|^3}\\
&\qquad\qquad-\frac{3\mu}{4\pi(1-\nu)}\frac{(\mathbf{r}\cdot\mathbf{n}_s)^2(\tilde{\mathbf{n}}_d(\mathbf{X}^S)\cdot\mathbf{b})(\mathbf{r}\cdot\mathbf{b})}{\|\mathbf{r}\|^5}\Bigg]dS\\
&+\frac{\mu b^2}{4\pi(1-\nu)}\kappa\Bigg\{\big(1+\nu-3\nu\sin^2\beta\big)\log\frac{D}{2\pi r_c\|\tilde{\mathbf{n}}_d\|}-\frac{3}{2}+\frac{\nu}{2}+\left(\frac{5}{4}-\frac{\nu}{2}\right)\sin^2\beta\\
&\qquad\qquad+[3-\nu+(-1+\nu)\sin^2\beta]\|\tilde{\mathbf{n}}_d\|^2-2\|\tilde{\mathbf{n}}_d\|^4\sin^2\beta\Bigg\}\\
&+\frac{\mu b^2}{4\pi(1-\nu)}\frac{\kappa_n}{\|\tilde{\mathbf{n}}_d\|}\Bigg\{(-1+\nu-\nu\sin^2\beta)+[2-2\nu+(6+2\nu)\sin^2\beta]\|\tilde{\mathbf{n}}_d\|^2-8\sin^2\beta\|\tilde{\mathbf{n}}_d\|^4\Bigg\}\\
&+\frac{\mu b^2}{\pi(1-\nu)}\left(\frac{\partial^2\mathbf{X}^S}{\partial\mathbf{t}^0\partial\mathbf{n}_s}\bigg|_{\mathbf{X}}\cdot\mathbf{n}^0\right)(\mathbf{n}_{\text{surface}}\cdot\mathbf{n}_s)\sin\beta\cos\beta(-\nu\|\tilde{\mathbf{n}}_d\|+2\|\tilde{\mathbf{n}}_d\|^3),
\end{aligned}\tag{4.37}$$

where S is the dislocation array surface with dislocations being the intersection of S with planes normal to the z axis, $\mathbf{X}$ is a point on the surface S where the force is evaluated, $\mathbf{X}^S$ is the point that varies on the surface S, $\mathbf{r}=\mathbf{X}-\mathbf{X}^S$, $\mathbf{n}_{\text{surface}}$ is the unit normal vector of the dislocation array surface S, $\mathbf{n}_s$ is the unit normal vector of the slip planes of the dislocations, $\tilde{\mathbf{n}}_d$ is the component of $\mathbf{n}_{\text{surface}}$ in the normal direction of the constituent dislocation given in equation (3.2), $\mathbf{t}^0$ is the unit tangent vector of the dislocation, $\mathbf{n}^0$ is the unit normal vector of the dislocation, $\mathbf{b}$ is the Burgers vector of the constituent dislocations, D is the distance between two adjacent slip planes of the dislocations, β is the angle between the dislocation line direction and the Burgers vector $\mathbf{b}$, κ is the curvature of the dislocation, κ_n is the normal curvature of the dislocation array surface S in the direction perpendicular to the dislocation, and r_c is a parameter depending on the dislocation core given in equation (3.3).

The continuum approximation in equation (4.37) is accurate up to two orders of b. The integral term in it gives the long-range interaction of dislocations in the array, and the other local terms give corrections at the next order. The local terms containing the dislocation curvature κ come from the line tension effect of the dislocations. The local terms containing the normal curvature κ_n of the dislocation array surface represent the effect of the variation of the dislocation array surface in the direction perpendicular to the dislocation. The local terms in the last line of equation (4.37) are associated with the variation of the dislocation line direction normal to the slip plane.

For the continuum model of the dynamics of the dislocation array surface, the velocity of the surface is determined from the continuum Peach-Koehler force by the mobility law in equation (3.4), following that of the discrete model in equation (2.10). Well-posedness of the continuum model will be examined in the next section by linear

stability analysis. It turns out that when we keep the leading order integral term (denoted as the $O(1)$ term), and the $O(b\log b)$ terms which are from the dislocation line tension effect, the continuum model is well-posed. For completeness of physics and increase of accuracy, we also keep those $O(b)$ terms from the dislocation line tension effect, and the resulting continuum model, as presented in equation (3.1) in Section 3, is also well-posed and is very accurate in the continuum regime, which will be shown in the next section. Whereas the complete asymptotic expansion up to $O(b)$ given in equation (4.37), unfortunately, will lead to ill-posedness in the continuum dynamics model.

5. Well-posed continuum model

In this section, by linear stability analysis of regular arrays of dislocations and comparisons with the results from the discrete model, we examine the well-posedness of the continuum dynamics model when the continuum Peach-Koehler force f in equation (3.1) or the complete continuum approximation f^c in equation (4.37) is incorporated.

We consider a regular array of straight edge dislocations forming a low angle symmetric tilt boundary ([33], Chap. 19 in [15], Chap. 2 in [41]). This dislocation array is subject to small perturbations of the constituent dislocations in their slip planes [36, 54]; see the schematic plot in figure 2.1. Assume that initially the regular array of dislocations form a plane located at $y=0$, and the constituent dislocations are in the slip planes $z=jD$, $j=\cdots,-2,-1,0,1,2,\cdots$, respectively. The Burgers vector of these constituent dislocations is $\mathbf{b}=(0,b,0)$. For a perturbation of amplitude ε with wavenumber k_1 along the dislocations and phase shift α for different dislocations, the constituent dislocations in the perturbed array can be written as $\gamma_j(t)=(x,\varepsilon e^{ik_1x+ij\alpha+\omega(k_1,\alpha)t},jD)$, $j=\cdots,-2,-1,0,1,2,\cdots$, where $\omega(k_1,\alpha)$ is the growth rate of the amplitude of the perturbation.

The discrete model in equations (2.8) and (2.10), by keeping only the linear terms of ε, gives the following dispersion relation:

$$\begin{aligned}&\omega(k_1,\alpha)\\ &=\frac{M\mu b^2}{2\pi(1-\nu)}\sum_{j\neq 0}\left[-\frac{1}{j^2D^2}+\nu\cos(j\alpha)k_1^2K_0(|k_1||j|D)+\cos(j\alpha)\frac{|k_1|}{|j|D}K_1(|k_1||j|D)\right]\\ &\quad+\frac{M\mu b^2}{2(1-\nu)}\int_0^{+\infty}\eta\delta(\eta)d\eta\left[(2\nu-1)k_1^2K_0(|k_1||\eta|)-\frac{1}{4}|\eta||k_1|^3K_1(|k_1||\eta|)\right],\end{aligned}\tag{5.1}$$

where K_0 and K_1 are the modified Bessel functions of the second kind.

We choose the Poisson ratio $\nu=\frac{1}{3}$. The distance between neighboring dislocations is $D=50b$. The regularized delta function that represents the dislocation core is $\delta(\eta,\psi)=\delta(\eta)=\frac{\pi}{(\pi^2-4)\eta_0^2}\left[1+\cos\left(\frac{\pi\eta}{\eta_0}\right)\right]$ if $0\le\eta\le\eta_0$ and 0 otherwise, where the width of the dislocation core is $\eta_0=3b$. The core parameter r_c in the continuum model is then $0.38\eta_0$ from equation (3.3).

In the continuum models, the perturbed tilt boundary can be written as $y=\varepsilon e^{ik_1x+ik_3z+\omega t}$, where k_1 and k_3 are frequencies of the perturbations along and normal to the constituent dislocations, respectively, with $k_3=\alpha/D$.

5.1. Well-posedness using the continuum Peach-Koehler force f.

We first examine the well-posedness of the continuum dynamics model when the continuum Peach-Koehler force f in equation (3.1) is used. Recall that f is obtained

by keeping the leading order integral term and the $O(b\log b)$ terms (relative to the leading order) which are from the dislocation line tension effect, together with other terms from dislocation line tension at $O(b)$. For convenience of expression, in this section, the continuum force f is referred to as the modified continuum force.

When incorporated into the evolution equation in equation (3.4), this modified continuum Peach-Koehler force f gives the following dispersion relation for this problem:

$$\omega(k_1,k_3)=\frac{M\mu b^2}{4\pi(1-\nu)}\left\{-\frac{2\pi}{D}\frac{(1-\nu)k_1^2+k_3^2}{\sqrt{k_1^2+k_3^2}}-\left[(1-2\nu)\log\frac{D}{2\pi r_c}-\frac{1}{4}\right]k_1^2\right\}. \tag{5.2}$$

The $O(\sqrt{k_1^2+k_3^2})$ term in this dispersion relation comes from the integral term in f which represents the long-range interaction of dislocations. The $O(k_1^2)$ term comes from the dislocation curvature κ term in f which is due to the dislocation line tension effect, and has a negative sign due to the assumption that D/b is a large finite number (low angle grain boundary). The fact that both the $O(\sqrt{k_1^2+k_3^2})$ and $O(k_1^2)$ terms have negative sign shows well-posedness of the continuum model in this problem.

The comparisons of the dispersion relation in equation (5.2) from the modified continuum Peach-Koehler force f with the dispersion relation in equation (5.1) from the discrete model are shown in figure 5.1.

Figure 5.1(a) shows the dispersion relations when the perturbation is normal to the constituent dislocations. In this case, the dislocations remain straight, i.e., $k_1=0$, and the dispersion relation in equation (5.1) from the discrete model can be calculated as $\omega(0,\alpha)=-\frac{M\pi\mu b^2}{(1-\nu)D^2}\left(\frac{1}{n}-\frac{1}{n^2}\right)$, where $n=2\pi/\alpha$ is the number of dislocations in one perturbation period normal to the dislocations. From the discrete model, the effect of the Peach-Koehler force always stabilizes the tilt boundary, i.e., the growth rate of the amplitude of the perturbation $\omega<0$. The resulting dispersion relation in equation (5.2) of the continuum model in this case is $\omega(0,k_3)=-\frac{M\mu b^2}{2D(1-\nu)}|k_3|$, which gives stability that agrees quantitatively with the result of the discrete model for not small n and qualitatively in the discrete limit of small n; see figure 5.1(a).

The dispersion relations when the perturbation is along the constituent dislocations, i.e. $\alpha=0$ and $k_3=0$, are shown in figure 5.1(b). The effect of the Peach-Koehler force always stabilizes the tilt boundary from the discrete model. It can be seen from the figure that our continuum approximation gives accurate results compared with those of the discrete model.

In this case, in the continuum Peach-Koehler force f in equation (3.1), in addition to the leading order long-range interaction of dislocations, the dislocation curvature terms from the local line tension effect of dislocations also contribute to the stability effect and give the negative $O(k_1^2)$ term in the dispersion relation in equation (5.2). To see the importance of the dislocation curvature terms in the continuum approximation, we also plot the dispersion relation of the leading order continuum approximation without curvature terms in figure 5.1(b). It can be clearly seen from the figure that without the dislocation curvature terms, the error of the continuum approximation in the dispersion relation is large for large k_1. Therefore it is crucial to include the dislocation curvature terms in the continuum model. The curvature terms are also crucial to incorporate in the continuum model the transition from the long-range interaction dominant regime to the curvature dominant regime (see [54]) and the size dependent effect (to be shown in the next section) as the length scale decreases.

Figure 5.1 (d) shows the full dispersion relation in equation (5.2) from the modified continuum Peach-Koehler force f, which is compared with that in equation (5.1) from

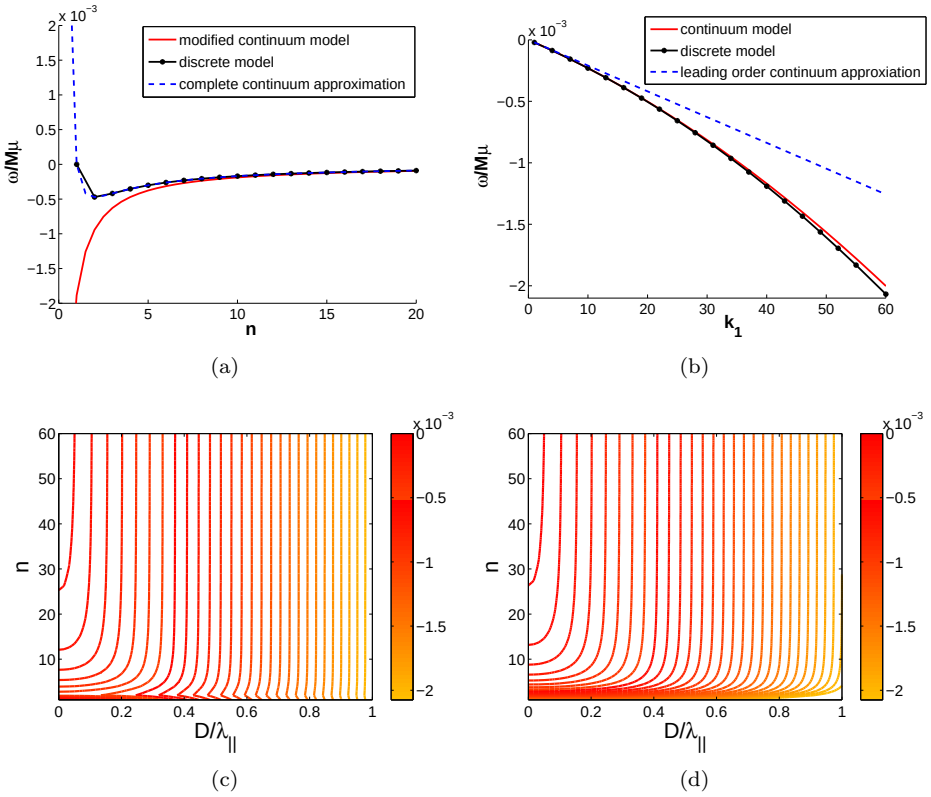

FIG. 5.1. *The dispersion relations for a perturbed symmetric tilt boundary consisting of edge dislocations. (a) The perturbation is normal to the constituent dislocations with n dislocations in one period. (b) The perturbation is along the constituent dislocations with wavenumber k_1. (c) The full dispersion relation from the discrete dislocation model. (d) The full dispersion relations from the modified continuum model. Here $n=2\pi/\alpha$ is the number of dislocations in one perturbation period normal to the dislocations, and $\lambda_{\|}=2\pi/k_1$ is the wavelength of the perturbation along the dislocations. The distance between neighboring dislocation is $D=50b$. The size of the domain is $L=3000b$.*

the discrete model shown in figure 5.1 (c). It can be seen that this continuum model gives a more accurate dispersion relation compared with the discrete model, except in the discrete limit where only a few dislocations are contained in the unit area; in the latter case, the continuum model is able to give qualitative stability.

5.2. Ill-posedness using the full continuum Peach-Koehler force f^c. When the full continuum Peach-Koehler force f^c in equation (4.37) is used, together with equation (3.4), we obtain the dispersion relation

$$\omega(k_1,k_3)=\frac{M\mu b^2}{4\pi(1-\nu)}\left\{-\frac{2\pi}{D}\frac{(1-\nu)k_1^2+k_3^2}{\sqrt{k_1^2+k_3^2}}-\left[(1-2\nu)\log\frac{D}{2\pi r_c}-\frac{1}{4}\right]k_1^2+k_3^2\right\}. \quad (5.3)$$

The additional $O(k_3^2)$ term (compared with the dispersion relation in equation (5.2) from the modified continuum force f) comes from the κ_n terms in f^c which are associated with the normal curvature of the dislocation array surface S in the direction on S perpendicular to the local dislocation line direction. This $O(k_3^2)$ term in the

dispersion relation has a positive sign, resulting in instability for large values of k_1 (small values of $n=2\pi/k_3D$) which is in contradiction with the stability results of the discrete model; see figure 5.1(a). Thus the κ_n terms in the full continuum Peach-Koehler force f^c in equation (4.37) lead to unphysical instability and ill-posedness of the continuum model.

The terms due to the variation of the dislocation line direction normal to the slip planes in the continuum Peach-Koehler force f^c in the last line in equation (4.37) make no contribution to the dispersion relation in the linear stability of a symmetric tilt boundary discussed above. To examine the well-posedness effect of these terms in the continuum model, we consider a dislocation array surface $y=cz$ with Burgers vector $\mathbf{b}=(b_1,b_2,0)$ subject to small perturbations: $y=cz+\varepsilon e^{ik_1x+ik_3z+\omega t}$. Then the contribution to the dispersion relation from these terms due to the variation of dislocation line direction normal to the slip planes are

$$\omega_3=\frac{M\mu b^2}{4\pi(1-\nu)}k_1k_3\left[-\frac{4\nu c}{1+c^2}+\frac{8c}{(1+c^2)^2}\right]\sin\beta\cos\beta. \tag{5.4}$$

Except for the special cases of $c=0$, $\sin\beta=0$, or $\cos\beta=0$, ω_3 is always positive for certain ranges of large values of k_3 and is at the highest order ($O(k_1^2+k_3^2)$ of the dispersion relation), thus this contribution also leads to ill-posedness of the continuum evolution equation.

5.3. Summary of well-posed continuum model. The modified continuum Peach-Koehler force f containing the leading order long-range dislocation interaction and terms due to the dislocation line tension effect gives a well-posed continuum model and is seen to be very accurate compared with the discrete model by linear stability analysis. Whereas the other two contributions in the full continuum Peach-Koehler force f^c, namely the contribution from the normal curvature of the dislocation array surface S in the direction on S perpendicular to the local dislocation line direction and that from the variation of dislocation line direction normal to the slip planes, lead to ill-posedness of the continuum model.

Alternatively, one can seek even higher order terms to stabilize the evolution equation to keep the later two contributions. However, this will make the expression extremely complicated and will involve even higher derivatives, resulting in severe stability restrictions on the time steps (the CFL condition) in numerical simulations. Thus this solution is not feasible in practice.

6. Accuracy of the continuum model and the size-dependent effect

In this section, beyond linear stability of planar dislocation arrays, we further examine the accuracy of the modified continuum Peach-Koehler force f in equation (3.1) via dislocation array structures that may form by interactions with particles and have been studied using discrete dislocation models [14, 34, 8, 31]. We focus on the accuracy as well as the size-dependent effect [28, 2, 9, 35, 29, 13, 1, 4, 12, 39, 50, 40, 18, 46, 53].

We consider an example of an array of dislocation loops surrounding a spherical particle; see figure 6.1(a). The distance between adjacent dislocation loops is $D=50b$, and the radius of the sphere is $R=ND$ for an integer N. There are a total of $2N-1$ dislocation loops and the middle one is in the plane containing the sphere center. We consider the Peach-Koehler force on an edge point on the dislocation loop with height $R/2$ from the sphere center; see figure 6.1(a).

The results using the continuum model f and comparisons with the results from the discrete model f^d are shown in figure 6.1(b). The Poisson ratio $\nu=1/3$ and the

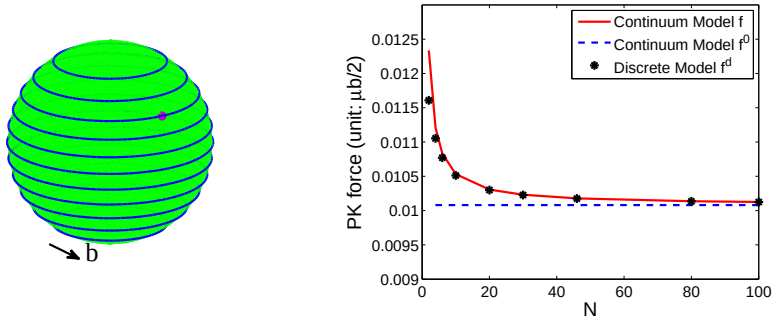

(a) (b)

FIG. 6.1. *(a) An array of dislocation loops surrounding a spherical particle. The dot on the surface indicates the location where the Peach-Koehler force is evaluated. The distance between adjacent dislocation loops is $D=50b$, and the radius of the sphere is $R=ND$ for an integer N. (b) The Peach-Koehler force using different models when the size of the particle varies.*

dislocation core profile is the same as that in the previous section. The radius of the sphere $R=ND$ sets the length scale of the continuum model: as the parameter N varies from 2 to 100, the length unit R in the continuum model varies from $100b$ to $5000b$. It can be seen that the continuum model f in equation (3.1) is very accurate as an approximation to the discrete model f^d in equation (2.8), and gives the correct size effect as the length unit of the continuum model decreases. On the other hand, the leading order continuum approximation f^0 in equation (4.6) has relatively large error, especially when the length unit of the continuum model is not very large, and is size independent.

7. Generalization to elastic anisotropy

In this section, we discuss the generalization of our continuum model to dislocation arrays in an elastically anisotropic medium. For this purpose, we write the continuum Peach-Koehler force in an isotropic medium in equation (3.1) as

$$f(\mathbf{X})=\frac{1}{D}\int_S\left[\frac{\mu b^2}{4\pi}\frac{\mathbf{r}\cdot\tilde{\mathbf{n}}_d(\mathbf{X}^S)}{\|\mathbf{r}\|^3}+\frac{\nu\mu}{4\pi(1-\nu)}\frac{(\tilde{\mathbf{n}}_d(\mathbf{X}^S)\cdot\mathbf{b})(\mathbf{r}\cdot\mathbf{b})}{\|\mathbf{r}\|^3}\right.$$
$$\left.-\frac{3\mu}{4\pi(1-\nu)}\frac{(\mathbf{r}\cdot\mathbf{n}_s)^2(\tilde{\mathbf{n}}_d(\mathbf{X}^S)\cdot\mathbf{b})(\mathbf{r}\cdot\mathbf{b})}{\|\mathbf{r}\|^5}\right]dS$$
$$+\frac{\mu b^2}{4\pi(1-\nu)}\left(1+\nu-3\nu\sin^2\beta\right)\kappa\log\frac{D}{2\pi\tilde{r}_c(\beta,\tilde{\mathbf{n}}_d)\|\tilde{\mathbf{n}}_d\|}, \tag{7.1}$$

where $\tilde{r}_c(\beta,\tilde{\mathbf{n}}_d)$ is a function depending on the dislocation core and the orientations of the dislocation array surface, the constituent dislocation, and the Burgers vector. The pre-logarithm factor of the curvature term, $\frac{\mu b^2}{4\pi(1-\nu)}\left(1+\nu-3\nu\sin^2\beta\right)$, comes from the singular asymptotic behavior of the self stress; see equation (4.7) in Section 4 and [10, 52]. Inside the logarithm, $D/\|\tilde{\mathbf{n}}_d\|$ is the distance between adjacent dislocations in the array.

When the medium is elastically anisotropic, using the classical formula for the asymptotic behavior of the dislocation self force (equation (5.4) in [10]) and Mura's formula for the stress field of continuous distributions of dislocations (equation (37.13)

in Chap. 6 of [27]), we can write down the generalization of the continuum Peach-Koehler force in such a medium in the following form:

$$f(\mathbf{X}) = \int_S \sum_{k,l,p,q,m,n,h} (b_1 C_{13kl} + b_2 C_{23kl}) \epsilon_{lnk} C_{pqmn} \frac{\partial G_{kp}(\mathbf{r})}{\partial x_q} b_m t_h dS + [e_d(\beta) + e_d''(\beta)] \kappa \log \frac{D}{2\pi \tilde{r}_c(\beta, \tilde{\mathbf{n}}_d) \|\tilde{\mathbf{n}}_d\|}, \tag{7.2}$$

where the summations are taken for repeated indices. Here $\{G_{kp}(\mathbf{r})\}$ are the Green's functions (equation (3.22) in Chap. 1 of [27]), $\{C_{ijkl}\}$ are the elastic constants, ϵ_{lnk} is the permutation tensor, which is 1 when $lnk = 123, 231, 312$, -1 when $lnk = 132, 213, 321$, and 0 otherwise, $\mathbf{t} = (t_1, t_2, 0)$ is the unit tangent vector of the dislocation, and $e_c(\beta)$ is the orientation-dependent pre-logarithmic energy factor for an infinite straight dislocation in the elastically anisotropic medium.

The rigorous derivation of the above continuum model in an anisotropic medium can follow the same procedure as presented in Section 4 for an isotropic medium. However, it will be extremely complicated to obtain the exact expression of $\tilde{r}_c(\beta, \tilde{\mathbf{n}}_d)$ in an anisotropic medium and may require numerical evaluation. Rigorous verification or numerical calculation for such term will be considered in the future work.

8. Conclusions and discussion

We have derived a continuum model for the dynamics of a dislocation array that consists of dislocations in different slip planes. In the continuum model, the dislocation array is represented by a continuous surface, of which there are many dislocations in a unit area at the scale of the continuum model. The continuum model is derived rigorously from the discrete model of the Peach-Koehler force on the constitutive dislocations in the array using asymptotic analysis. The obtained continuum force contains an integral over the surface representing the long-range interaction of dislocations in the array, and a local curvature term due to the line tension effect of dislocations. Well-posedness of the continuum model is examined by stability analysis of a regular array of straight dislocations. The size-dependent effect due to dislocation line tension is accurately incorporated in the continuum model. Generalizations to anisotropic elasticity are discussed.

By asymptotic analysis, we have also obtained other higher order local terms in the continuum formulation for the interactions of dislocations in a dislocation array. These terms represent the local effects of dislocations normal to the slip planes, including the normal curvature of the dislocation array surface in the direction on the surface perpendicular to the local dislocation and the variation of the dislocation line direction in the normal direction of the slip plane; see equation (4.37). These higher order terms are not able to be included in our continuum model for the dynamics of dislocation arrays due to the requirements of well-posedness. However, they are still very important for further understanding of dislocation interactions at the continuum level. For example, they provide mathematical insight for the fact that some available continuum theories with higher order terms with similar physical origins (dislocation correlations) derived from stochastically distributed dislocations [12] do not apply generally to deterministic arrangements of dislocations such as dislocation arrays [37].

The continuum model derived in this paper applies to dislocation arrays that consist of dislocations in equidistant slip planes with the same Burgers vector. Continuum models for dislocation arrays that consist of dislocations with multiple Burgers

vectors and dislocations in non-equidistant slip planes, which are associated with dislocation climb, are being studied and the results will be reported elsewhere. Some other physical implications of the continuum model have been published in [54].

REFERENCES

[1] A. Acharya, *A model of crystal plasticity based on the theory of continuously distributed dislocations*, J. Mech. Phys. Solids, 49, 761–784, 2001.

[2] E.C. Aifantis, *On the dynamical origin of dislocation patterns*, Mater. Sci. Eng., 81, 563–574, 1986.

[3] A. Arsenlis, W. Cai, M. Tang, M. Rhee, T. Oppelstrup, G. Hommes, T.G. Pierce, and V.V. Bulatov, *Enabling strain hardening simulations with dislocation dynamics*, Modelling Simul. Mater. Sci. Eng., 15, 553–595, 2007.

[4] A. Arsenlis and D.M. Parks, *Modeling the evolution of crystallographic dislocation density in crystal plasticity*, J. Mech. Phys. Solids, 50, 1979–2009, 2002.

[5] C.J. Ball, *Surface distributions of dislocations in metals: II*, Phil. Mag., 2, 977–984, 1957.

[6] C.J. Ball and P.B. Hirsch, *Surface distributions of dislocations in metals*, Phil. Mag., 7, 1343–1352, 1955.

[7] J.W. Cahn, Y. Mishin, and A. Suzuki, *Coupling grain boundary motion to shear deformation*, Acta Mater., 54, 4953–4975, 2006.

[8] K.T. Chu, D.J. Srolovitz, and Y. Xiang, *Level set method approaches to dislocation models of grain boundaries*, minisymposium presentation at SIAM Conference on Analysis of Partial Differential Equations, 2006.

[9] N.A. Fleck and J.W. Hutchinson, *A phenomenological theory for strain gradient effects in plasticity*, J. Mech. Phys. Solids, 41, 1825–1857, 1993.

[10] S.D. Gavazza and D.M. Barnett, *The self-force on a planar dislocation loop in an anisotropic linear-elastic medium*, J. Mech. Phys. Solids, 24, 171–185, 1976.

[11] N.M. Ghoniem, S.H. Tong, and L.Z. Sun, *Parametric dislocation dynamics: A thermodynamics-based approach to investgations of mesoscopic plastic deformation*, Phys. Rev. B, 61, 913–927, 2000.

[12] I. Groma, F.F. Csikor, and M. Zaiser, *Spatial correlations and higher-order gradient terms in a continuum description of dislocation dynamics*, Acta Mater., 51, 1271–1281, 2003.

[13] M.E. Gurtin, *On plasticity of crystals: Free energy, microforces, plastic strain gradients*, J. Mech. Phys. Solids, 48, 989–1036, 2000.

[14] J. Hirth, *A model for a propagating shear band on the basis of a tilt wall dislocation array*, Appl. Mech. Rev., 45, S71–S74, 1992.

[15] J. Hirth and J. Lothe, *Theory of Dislocations*, Wiley, New York, 2nd ed., 1982.

[16] U. Kocks, T. Hasegawa, and R. Scattergood, *On the origin of cell walls and of lattice misorientations during deformation*, Scripta Metall., 14, 449–454, 1980.

[17] A. Kosevich, *Crystal dislocations and the theory of elasticity*, in Dislocations in Solids, F. Nabarro, ed., North-Holland, Amsterdam, 1, 33–141, 1979.

[18] J. Kratochvíl and R. Sedláček, *Statistical foundation of continuum dislocation plasticity*, Phys. Rev. B, 77, 134102, 2008.

[19] L.P. Kubin, G. Canova, M. Condat, and B. Devincre, *Dislocation microstructures and plastic flow: A 3d simulation*, Solid State Phenomena, 23/24, 455–472, 1992.

[20] R.W. Lardner, *Mathematical Theory of Dislocations and Fracture*, University of Toronto Press, Toronto, 1974.

[21] C. Li, E. Edwards, J. Washburn, and E. Parker, *Stress-induced movement of crystal boundaries*, Acta Metall., 1, 223–229, 1953.

[22] P. Li, Z. Zhang, S. Li, and Z. Wang, *Comparison of dislocation patterns in cyclically deformed fcc metals*, Scripta Mater., 59, 730–733, 2008.

[23] A.T. Lim, D.J. Srolovitz, and M. Haataja, *Low-angle grain boundary migration in the presence of extrinsic dislocations*, Acta Mater., 57, 5013–5022, 2009.

[24] J. Lothe, *Dislocations in continuous elastic media*, in Elastic Strain Fields and Dislocation Mobility, V. L. Indenbohm and L. Lothe, eds., North-Holland, Amsterdam, 175–235, 1992.

[25] H. Mughrabi, *Dislocation wall and cell structures and long-range internal stresses in deformed metal crystals*, Acta Metall., 31, 1367–1379, 1983.

[26] H. Mughrabi, F. Ackermann, and K. Herz, *Persistent slip bands in fatigued face-centred and body-centred cubic metals*, in Fatigue Mechanisms, ASTM STP 675, J. Fong, ed., American Society for Testing and Materials, Philadelphia, 69–105, 1979.

[27] T. Mura, *Continuous distribution of moving dislocations*, Phil. Mag., 89, 843–857, 1963.

[28] D. Nelson and J. Toner, *Bond-orientational order, dislocation loops, and melting of solids and smectic-a liquid crystals*, Phys. Rev. B, 24, 363–387, 1981.
[29] W.D. Nix and H. Gao, *Indentation size effects in crystalline materials: A law for strain gradient plasticity*, J. Mech. Phys. Solids, 46, 411–425, 1998.
[30] M. Peach and J. S. Koehler, *The forces exerted on dislocations and the stress fields produced by them*, Phys. Rev., 80, 436–439, 1950.
[31] S.S. Quek, Y. Xiang, and D.J. Srolovitz, *Loss of interface coherency around a misfitting spherical inclusion*, Acta Mater., 59, 5398–5410, 2011.
[32] D. Raabe, *3d simulation of the stress fields associated with disorderred finite dislocation walls in face centred cubic crystals*, Comput. Mater. Sci., 4, 143–150, 1995.
[33] W. Read and W. Shockley, *Dislocation models of crystal grain boundaries*, Phys. Rev., 75, 275–289, 1950.
[34] M. Rhee, J. Hirth, and H. Zbib, *A superdislocation model for the strengthening of metal matrix composities and the initiation and propagation of shear bands*, Acta Metall. Mater., 42, 2645–2655, 1994.
[35] J.M. Rickman and J. Vinals, *Modelling of dislocation structures in materials*, Phil. Mag. A, 75, 1251–1262, 1997.
[36] C. Rottman, *Thermal fluctuations in low-angle grain boundaries*, Acta Metall. Mater., 34, 2465–2470, 1986.
[37] A. Roy, R.H.J. Peerlings, M.G.D. Geers, and Y. Kasyanyuk, *Continuum modeling of dislocation interactions: Why discreteness matters*, Mater. Sci. Eng. A, 486, 653–661, 2008.
[38] G. Saada and E. Bouchaud, *Dislocation walls*, Acta Metall. Mater., 41, 2173–2178, 1993.
[39] R. Sedláček, J. Kratochvíl, and E. Werner, *The importance of being curved: Bowing dislocations in a continuum description*, Phil. Mag., 83, 3735–3752, 2003.
[40] R. Sedláček, C. Schwarz, J. Kratochvíl, and E. Werner, *Continuum theory of evolving dislocation fields*, Phil. Mag., 87, 1225–1260, 2007.
[41] A. Sutton and R. Balluffi, *Interfaces in Crystalline Materials*, Clarendon Press, Oxford, 1995.
[42] J. Washburn and E. Parker, *Kinking in zinc single-crystal tension specimens*, Trans. AIME, 194, 1076–1078, 1952.
[43] W. Webb, *The interaction of solutes with dislocation walls*, Acta Metall., 5, 89–96, 1957.
[44] M. Winning, G. Gottstein, and L. S. Shvindlerman, *On the mechanisms of grain boundary migration*, Acta Mater., 50, 353–363, 2002.
[45] Y. Xiang, *Derivation of a continuum model for epitaxial growth with elasticity on vicinal surface*, SIAM J. Appl. Math., 63, 241–258, 2002.
[46] Y. Xiang, *Continuum approximation of the Peach-Koehler force on dislocations in a slip plane*, J. Mech. Phys. Solids, 57, 728–743, 2009.
[47] Y. Xiang, L.T. Cheng, D.J. Srolovitz, and W. E, *A level set method for dislocation dynamics*, Acta Mater., 51, 5499–5518, 2003.
[48] Y. Xiang and W. E, *Misfit elastic energy and a continuum model for epitaxial growth with elasticity on vicinal surfaces*, Phys. Rev. B, 69, 035409, 2004.
[49] H. Xu and Y. Xiang, *Derivation of a continuum model for the long-range elastic interaction on stepped epitaxial surfaces in 2+1 dimensions*, SIAM J. Appl. Math., 65, 1393–1414, 2009.
[50] M. Zaiser and T. Hochrainer, *Some steps towards a continuum representation of 3d dislocation systems*, Scripta Mater., 54, 717–721, 2006.
[51] H.M. Zbib, M. Rhee, and J.P. Hirth, *On plastic deformation and the dynamics of 3d dislocations*, Int. J. Mech. Sci., 40, 113–127, 1998.
[52] D. Zhao, H. Wang, and Y. Xiang, *Asymptotic behaviors of the stress fields in the vicinity of dislocations and dislocation segments*, Phil. Mag., to appear, 2012.
[53] X. Zhu and Y. Xiang, *Continuum model for dislocation dynamics in a slip plane*, Phil. Mag., 90, 4409–4428, 2010.
[54] X. Zhu and Y. Xiang, *Stabilizing force on perturbed grain boundaries using dislocation model*, Scripta Mater., 64, 5–8, 2011.
[55] X. Zhu, H. Xu, and Y. Xiang, *Continuum model for the long-range elastic interaction on stepped epitaxial surfaces in* $2+1$ *dimensions*, Phys. Rev. B, 79, 125413, 2009.